

# Geometrically general scaling relations for locomotion on granular beds

James Slonaker<sup>1</sup>, D. Carrington Motley<sup>1</sup>, Carmine Senatore<sup>1</sup>, Karl Iagnemma<sup>1</sup>, Ken Kamrin<sup>1,\*</sup>

<sup>1</sup>*Department of Mechanical Engineering, MIT, Cambridge, MA 02139, USA*

(Dated: August 5, 2022)

Inspired by hypotheses of Resistive Force Theory, we have discovered a general dimensionless form for granular locomotion, which instructs how to scale size, mass, and driving parameters to relate dynamic behaviors of different locomotors in the same granular media. We experimentally confirm these scalings with wheel pairs of various shapes and sizes under many driving conditions in a common sand bed. We explain how the relations may be derived alternatively by assuming Coulombic yielding, and how the relations can be augmented to predict wheel performance in different ambient gravities.

Due to the complexity of the constitutive behavior of granular media [1] dynamic interactions between grains and solid bodies are challenging to model without resorting to grain-by-grain discrete particle methods. A recent approach to simplify these interactions is Resistive Force Theory (RFT) [2]. RFT is an empirical framework utilizing a set of hypotheses about local drag to approximate resistance on general solid surfaces moving in homogeneous granular soils near the surface. RFT was initially developed for viscous drag problems [3], however it has shown surprising effectiveness in granular media, where it has been used to simulate the dynamics of legged reptiles and robots [2], swimming sandfish [4], and the distribution of lift forces on curved submerged bodies in granular beds [5].

In light of its effectiveness in multiple geometries and its dependence on very few model parameters, a natural question to ask is whether RFT, when combined with Newton’s laws of motion, produces a set of intruder dynamics possessing fundamental invariances. If these could be identified and validated experimentally, they would provide a physical basis to directly relate different granular locomotion problems in the same soil, without the need to actually perform RFT simulation. In application, they could be exploited as scaling laws to predict the performance of a “large” locomotor in a sand bed, such as a treaded truck wheel or a tank’s caterpillar tracks, by appropriately down-scaled analysis of a smaller locomotor in the same bed, analogous to scaling techniques in fluid mechanics.

In this letter, we analyze arbitrarily shaped wheels as shown in Fig 1, and derive and validate a large family of geometrically-general scaling laws inspired by invariances within the RFT-based terradynamical system. The analysis could be applied to other locomotors with more moving parts, but we test on solid wheels here because they have few internal degrees of freedom, simplifying the analysis. Granular RFT is concerned solely with computing the resistance on a body moving through a gravitationally loaded bed of grains. It does not attempt to describe the flow or stress fields of the grains induced by the moving body. Its basic premise, which is not actually

derived physically (though new efforts are being made to provide its foundations [6]), is that a simple form governs the stress distribution that grains apply along the leading surface of a moving intruder.

Assume an intruder which moves in the  $xz$ -plane (gravity points in  $-\hat{z}$  direction,  $z = 0$  represents the sand surface) whose shape is quasi-2D also within the  $xz$ -plane. For  $S$  the leading surface of the intruder, the resistive force  $\mathbf{F}_{\text{res}} = (f_x, f_z)$  is modeled as

$$\mathbf{F}_{\text{res}} = \int_S (\alpha_x(\beta, \gamma), \alpha_z(\beta, \gamma)) H(z) |z| dA_s \quad (1)$$

where  $dA_s$  is the area,  $\beta$  is the surface element’s angle of tilt, and  $\gamma$  is the angle of the velocity of the surface element. Both  $\beta$  and  $\gamma$  are measured from the horizontal. The Heaviside function,  $H(z)$ , removes resistive force on parts of the intruder outside the bed, and the dependence on  $|z|$  is added to model increased resistance with depth due to gravity. The presumed independence of the local surface stress on the shape and motion of the other parts of the surface is an unproven assumption of the model, as is the assumption of linear variation of stress with  $z$ ; during intrusion, significant variation from a lithostatic pressure distribution is observed [7, 8].

The key constitutive ingredient in the model is the selection of the two functions  $\alpha_x$  and  $\alpha_z$ , which is done empirically by fitting experimental force data from intruding flat plates under various  $\beta$  and  $\gamma$  conditions. By comparing the experimental data for many granular materials it was observed [2] that the  $\alpha_{x,z}$  functions have a fairly common shape, supporting the approximation  $\alpha_{z,x}(\beta, \gamma) \approx \xi \alpha_{z,x}^{\text{gen}}(\beta, \gamma)$  where  $\alpha_{z,x}^{\text{gen}}$  are fixed dimensionless functions, and  $\xi$  is a force/volume quantity denoted the “grain-structure coefficient,” which depends on the surface physics of the solid, the mechanical properties of the particular granular media at hand, and the value of gravity. In this way,  $\xi$  is the only material parameter needed to execute an RFT calculation in locomotion.

By contrast, common engineering terradynamics models such as the model proposed by Wong and Reece (based on Bekker’s work) [9] or the NATO Reference Mobility Model [10] require a much larger number of

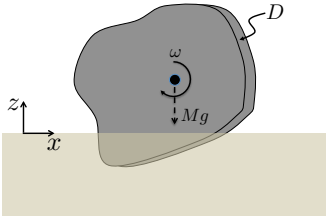


Figure 1: General problem: Driving an arbitrarily shaped wheel of width  $D$  and rotational velocity  $\omega$ , carrying a mass  $M$  under gravity  $g$ .

fit parameters, though they model more than resistive forces. Similarly, unlike the Bekker method [11], no knowledge of the material deformation is required.

*Dimensional analysis:* The generic wheel has a dimensionless shape, which we denote by a point-set  $f$ , a constant width  $D$  into the plane, a characteristic length  $L$  that scales the shape  $f$  to give the actual wheel cross-section, and a mass  $M$  assumed concentrated on the axle. The wheel is given a fixed rotational velocity  $\omega$ , is acted upon by some gravity  $g$ , and interacts with the sand bed through some grain-structure coefficient  $\xi$ . The outputs we are interested in are the power expended to drive the wheel through the grains,  $P$ , and the wheel's  $x$ -translational velocity  $V$ , although other outputs could be considered. Before applying dimensional analysis, note that by using  $\alpha_{z,x} = \xi \alpha_{z,x}^{\text{gen}}$  in Eq 1, the problem's dependence on  $\xi$  and  $D$  is seen only through the product  $\xi D$ . With this and a standard nondimensionalization, the wheel's steady driving limit-cycle is predicted to obey the form:

$$\left[ \frac{P}{Mg\sqrt{Lg}}, \frac{V}{\sqrt{Lg}} \right] = \Psi \left( \sqrt{\frac{g}{L}} t, f, \frac{g}{L\omega^2}, \frac{\xi DL^2}{Mg} \right) \quad (2)$$

where, for clarity,  $\Psi$  is a four-input, two-output function as shown. If the gravity, wheel surface texture, and granular media are fixed,  $g$  and  $\xi$  can be absorbed into the function, giving the reduced form:

$$\left[ \frac{P}{M\sqrt{L}}, \frac{V}{\sqrt{L}} \right] = \tilde{\Psi} \left( \sqrt{\frac{1}{L}} t, f, \frac{1}{L\omega^2}, \frac{DL^2}{M} \right) \quad (3)$$

The above forms give the following family of scaling relations: Consider two experiments with the same  $f$ ,  $g$ , and  $\xi$ , but one has inputs  $(L, M, D, \omega)$  and the other has inputs  $(L', M', D', \omega') = (rL, sM, sr^{-2}D, r^{-1/2}\omega)$  for any positive scalars  $r$  and  $s$ . Then the corresponding driving cycles should obey  $\langle P' \rangle = sr^{1/2} \langle P \rangle$  and  $\langle V' \rangle = r^{1/2} \langle V \rangle$  where  $\langle \cdot \rangle$  denotes a time-average.

*Connection to Coulomb plasticity:* Although RFT is empirical, interestingly, Eq 3 can also be deduced mechanically by considering wheel motion in a 3D bed of ideal Coulomb material [12]. Here, the grains are treated as

a rate-independent frictionally yielding continuum. Such a model could be used to predict the entire sand motion field, but instead consider dimensional analysis implications that can be identified without solving for flow. In this model, the wheel inputs remain the same, there is no grain structure coefficient  $\xi$ , and there are three granular material parameters: the density of the material  $\rho$ , the material's coefficient of internal friction  $\mu$ , and the coefficient of sliding friction of the wheel-material interface  $\mu_w$ . Wheels driving through this hypothetical continuum must obey the following dimensionless form:

$$\left[ \frac{P}{Mg\sqrt{Lg}}, \frac{V}{\sqrt{Lg}} \right] = \Psi_{\text{Coul}} \left( \sqrt{\frac{g}{L}} t, f, \frac{g}{L\omega^2}, \frac{D}{L}, \frac{\rho L^3}{M}, \mu, \mu_w \right) \quad (4)$$

If the gravity, wheel roughness, and granular media are fixed, the values of  $g$ ,  $\rho$ ,  $\mu$ , and  $\mu_w$  can be absorbed into the function yielding the reduced form:

$$\left[ \frac{P}{M\sqrt{L}}, \frac{V}{\sqrt{L}} \right] = \bar{\Psi}_{\text{Coul}} \left( \sqrt{\frac{1}{L}} t, f, \frac{1}{L\omega^2}, \frac{D}{L}, \frac{L^3}{M} \right) \quad (5)$$

This can be further reduced, if it is assumed that granular motion under the wheel is approximately invariant in the out-of-plane dimension. In this case, if the mass  $M$  and width  $D$  of the wheel are scaled by some  $C_0$ , this would be identical to running  $C_0$  copies of the wheel side by side. The resulting power would be  $C_0 P$  and the velocity would remain unchanged. From Eq 5, this means  $\bar{\Psi}_{\text{Coul}}$  is unchanged under such a transformation, which constrains  $\bar{\Psi}_{\text{Coul}}$  to depend on  $M$  and  $D$  only through the ratio  $D/M$ , requiring  $\bar{\Psi}_{\text{Coul}}$  to depend on its last two inputs only through their product:

$$\left[ \frac{P}{M\sqrt{L}}, \frac{V}{\sqrt{L}} \right] = \tilde{\Psi}_{\text{Coul}} \left( \sqrt{\frac{1}{L}} t, f, \frac{1}{L\omega^2}, \frac{DL^2}{M} \right) \quad (6)$$

This form is identical to Eq 3. Therefore, the scalings implied by RFT can be derived from Coulomb plasticity if the flow under the wheel is assumed invariant in the out-of-plane dimension, per a wheel with large enough  $D$  relative to sinkage.

*Experiments:* To test the above scalings, an experimental sand bed in the MIT Robotic Mobility Group Lab [13] was used. The test apparatus, as shown in Fig 2, consists of a Lexan bin filled with Quikrete medium sand surrounded by an aluminum frame. Attached to the aluminum frame are two low friction rods, which are attached to the carriage and allow for horizontal motion. The carriage is also attached through low-friction vertical rods to the main platform to allow for vertical wheel motion. This allows the wheel to translate freely, e.g. non-circular wheels “bobble” in the vertical direction as they drive through the grains. The main platform is connected to a motor driven wheel. The wheels were printed

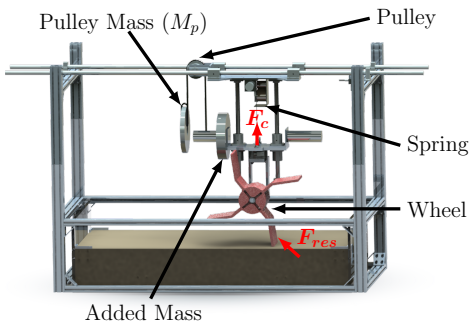


Figure 2: Experimental apparatus. The wheel rotates in the counter-clockwise direction. A constant force “spring” and a pulley are used to alter the wheel’s effective gravity.

in PLA plastic using a MakerBot 3D printer. Position, torque, velocity, and rotational velocity sensors are attached to the frame to record the relevant data.

Additionally, we developed a setup that allows us to vary the gravity felt by the wheel as shown in Fig 2. This lets us check the scalings resulting from Eq 2 under different selections of  $g$ , keeping  $\xi$  fixed. Lowering gravity also helps prevent overload of the wheel motor as mass increases. An SDP/SI Neg’ator constant-force “spring” ( $F_c = 66.7\text{N}$ ) is attached between the carriage and the main platform. A pulley is attached to the carriage platform and a belt around the pulley is attached to the main platform and a mass,  $M_p$ . The spring and pulley are used in tandem to vary the effective gravity on the wheel in a way that ensures the wheel’s gravitational and inertial masses always agree. This does not change the gravity experienced by the grains; hence the  $\xi$  value remains fixed. In view of Fig 2, the gravity change can be seen by applying Newton’s second law to the main carriage coupled to the hanging weight. The result is that the wheel’s translational motion always matches that of a free wheel whose mass is  $M = M_T + M_p$  and gravity is  $g = (M_T g_e - M_p g_e - F_c)/(M_T + M_p)$  where  $g_e$  is earth gravity and  $M_T$  is the total mass of the wheel, motor, main platform, and added mass.

Using these formulas for  $M$  and  $g$ , Equation 2 was tested rather exhaustively with a set of 288 experiments involving pairs of cylindrical wheels and four-arm lug wheels of varying size dimensions (defined in Fig 3), mass loadings, and rotation speeds. The cylindrical wheels are covered in sandpaper to increase interface friction, while not affecting the tested scaling relations. The lug wheels have four arms and have an elbow half way down their lengths bent to an angle of  $150^\circ$ .

The different test inputs are shown in Table I. In each test, a pair of wheels of the same geometrical family but different size dimensions were driven through the sand; one wheel is ‘big’ and one is ‘small’ as denoted with subscripts  $b$  and  $s$  in the table. Three pairs of wheels were used in total. For each pair, the two masses ( $M_b$  and  $M_s$ )



Figure 3: The two shapes,  $f$ , used in our study: cylinders (left) and lugs (right), and their corresponding definitions of  $L$ . The interior circle on the lug wheels was used for mounting and never came into contact with the sand.

Table I: Experimental tests performed and inputs used. Each row represents a different wheel pair for which 12 combinations of driving parameters were performed; mass and rotational velocity pairs represented as cartesian products.

	Common Parameters [cm], [cm], [m/s <sup>2</sup> ], [ ]	Driving Parameters [kg] x [deg/s]
Key	$\begin{bmatrix} L_b \\ L_s \end{bmatrix}, \begin{bmatrix} D_b \\ D_s \end{bmatrix}, [g], (\{\text{shape}\})$	$\begin{pmatrix} \begin{bmatrix} M_b^1 \\ M_s^1 \end{bmatrix} \begin{bmatrix} M_b^2 \\ M_s^2 \end{bmatrix} \begin{bmatrix} M_b^3 \\ M_s^3 \end{bmatrix} \\ \begin{bmatrix} \omega_b^1 \\ \omega_s^1 \end{bmatrix} \begin{bmatrix} \omega_b^2 \\ \omega_s^2 \end{bmatrix} \begin{bmatrix} \omega_b^3 \\ \omega_s^3 \end{bmatrix} \begin{bmatrix} \omega_b^4 \\ \omega_s^4 \end{bmatrix} \end{pmatrix} \times$
Pair A	$\begin{bmatrix} 12.50 \\ 8.08 \end{bmatrix}, \begin{bmatrix} 15 \\ 15 \end{bmatrix}, [3.71], (\{\text{Cyl}\})$	$\begin{pmatrix} \begin{bmatrix} 35.9 \\ 14.9 \end{bmatrix} \begin{bmatrix} 42.2 \\ 17.6 \end{bmatrix} \begin{bmatrix} 45.7 \\ 19.0 \end{bmatrix} \\ \begin{bmatrix} 14.0 \\ 17.4 \end{bmatrix} \begin{bmatrix} 17.0 \\ 21.2 \end{bmatrix} \begin{bmatrix} 20.0 \\ 24.9 \end{bmatrix} \begin{bmatrix} 23.0 \\ 28.6 \end{bmatrix} \end{pmatrix} \times$
Pair B	$\begin{bmatrix} 11.25 \\ 7.50 \end{bmatrix}, \begin{bmatrix} 14 \\ 14 \end{bmatrix}, [1.31], (\{\text{Lug}\})$	$\begin{pmatrix} \begin{bmatrix} 30.2 \\ 13.4 \end{bmatrix} \begin{bmatrix} 34.9 \\ 15.5 \end{bmatrix} \begin{bmatrix} 39.7 \\ 17.6 \end{bmatrix} \\ \begin{bmatrix} 14.0 \\ 17.1 \end{bmatrix} \begin{bmatrix} 17.0 \\ 20.8 \end{bmatrix} \begin{bmatrix} 20.0 \\ 24.5 \end{bmatrix} \begin{bmatrix} 23.0 \\ 28.2 \end{bmatrix} \end{pmatrix} \times$
Pair C	$\begin{bmatrix} 11.25 \\ 9.00 \end{bmatrix}, \begin{bmatrix} 14 \\ 10 \end{bmatrix}, [1.31], (\{\text{Lug}\})$	$\begin{pmatrix} \begin{bmatrix} 29.3 \\ 13.4 \end{bmatrix} \begin{bmatrix} 34.0 \\ 15.5 \end{bmatrix} \begin{bmatrix} 38.6 \\ 17.6 \end{bmatrix} \\ \begin{bmatrix} 14.0 \\ 15.6 \end{bmatrix} \begin{bmatrix} 17.0 \\ 19.0 \end{bmatrix} \begin{bmatrix} 20.0 \\ 22.4 \end{bmatrix} \begin{bmatrix} 23.0 \\ 25.7 \end{bmatrix} \end{pmatrix} \times$

and rotation speeds ( $\omega_b$  and  $\omega_s$ ) were chosen to ensure both big and small systems have the same dimensionless inputs to  $\Psi$ . That is, each pair of tests corresponded to two experiments where one relates to the other through a choice of the  $r$  and  $s$  scaling parameters described previously. The time-averaged non-dimensional power  $\langle \tilde{P} \rangle = \langle \frac{P}{Mg\sqrt{Lg}} \rangle$  and velocity  $\langle \tilde{V} \rangle = \langle \frac{V}{\sqrt{Lg}} \rangle$  were measured when the wheel motion reached cyclic behavior. In each case, the proposed scaling relation is satisfied if  $\langle \tilde{P}_b \rangle = \langle \tilde{P}_s \rangle$  and  $\langle \tilde{V}_b \rangle = \langle \tilde{V}_s \rangle$ .

The first tests performed were with cylindrical wheels (Pair A). The non-dimensional powers and velocities arising from each of the 12 pairs of driving parameters are plotted in Fig 4(a). Note that four repetitions of the same test are performed each time to obtain useful error-bars.

In general the expected trend is strongly observed at low rotational velocity, with some deviation at the highest rotational rate. The next series of tests utilized two four-arm lug wheels (Pair B). Again, the expected scaling relation is observed rather clearly (Fig 4(b)). The final series of experiments performed (Pair C) also used four-arm lug wheels, however the widths and lengths of the two wheels were not equal and not proportional. Hence, each test in this series involves two wheels with different lengths, widths, masses, and rotations — all differing by different factors — making this series the most stringent, and arguably most interesting, test of the proposed scaling relation. The agreement is quite strong (Fig 4(c)). The best-fit slopes of the six datasets in Fig 4 are all within 3% of our predicted value of 1.

From Eq 2, in addition to the time-average behaviors, the actual time-dependence of these quantities should relate when time is accordingly scaled. Figure 5 shows the non-dimensional power plotted against dimensionless time,  $\tilde{t} = \sqrt{\frac{g}{L}}t$ , over the course of a single cycle from two pairs of four-arm lug experiments in Pair C. The predicted agreement between trajectories is observed. The result is non-trivial; the dimensional powers differ by a factor of 2.45 for each pair.

*Potential extraplanetary applications:* It would be advantageous for future applications to extend the scalings arising from Eq 2 so that two experiments in the same sand but with different gravities can be related to each other; e.g. to use an earthbound experiment to predict an extraplanetary experiment. To do this correctly, one requires a theory to explain how  $\xi$  varies with gravity. Assuming an ideal Coulomb material, dimensional analysis implies that for a given sand,  $\xi$  takes the form

$$\xi = \rho g \hat{\xi}(\mu, \mu_w). \quad (7)$$

Therefore, to the extent that RFT is described by Coulomb plasticity theory, Eq 7 is a good approximation for the grain structure coefficient  $\xi$  from RFT.

By substituting Eq 7 into Eq 2, we obtain

$$\left[ \frac{P}{Mg\sqrt{Lg}}, \frac{V}{\sqrt{Lg}} \right] = \Psi \left( \sqrt{\frac{g}{L}}t, f, \frac{g}{L\omega^2}, \frac{\rho \hat{\xi}(\mu, \mu_w) DL^2}{M} \right) \quad (8)$$

With this new form, we obtain the following expanded scaling law to relate wheels in the same sand but under two different gravities: Consider two experiments with common  $f$ ,  $\rho$ ,  $\mu$ , and  $\mu_w$ , where one is described by the inputs  $(g, L, M, D, \omega)$  and the other by the inputs  $(g', L', M', D', \omega')$   $= (qg, rL, sM, sr^{-2}D, q^{1/2}r^{-1/2}\omega)$  for any positive scalars  $q$ ,  $r$ , and  $s$ . Then the steady driving cycles of the corresponding outputs should obey  $\langle P' \rangle = q^{3/2}r^{1/2}s\langle P \rangle$  and  $\langle V' \rangle = q^{1/2}r^{1/2}\langle V \rangle$ . When wheel pairs are properly scaled, this relation could be used to predict behaviors in different gravities [14].

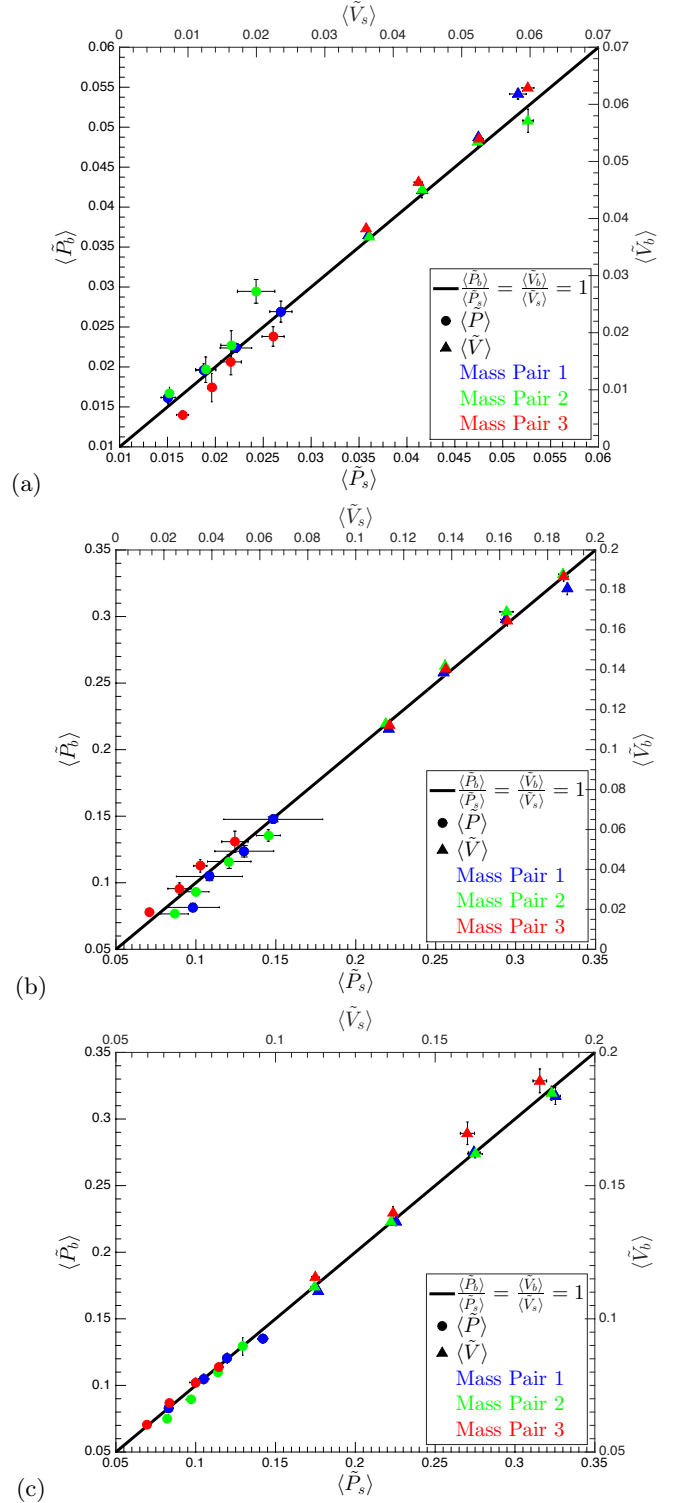


Figure 4: Time-average non-dimensional power and velocity values for Pair A (a), Pair B (b), and Pair C (c). Each color in each plot represents a different mass pair selection and the corresponding four points of each color represent different rotational velocity pairings. Model prediction is the solid line.

*Discussion:* We have proposed and experimentally validated a set of invariances in granular locomotion for the

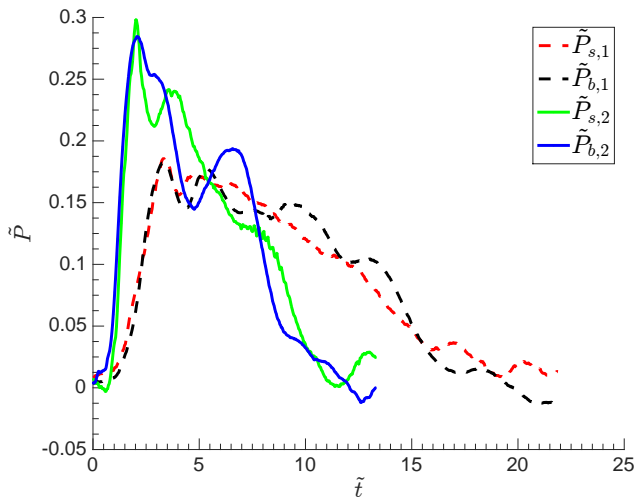


Figure 5: Non-dimensional power trajectories for two pairs of lug-wheel experiments over a single cycle ( $45^\circ$  of rotation). One pair is shown in green and blue solid lines, while the other is shown in black and red dotted lines.

case of rigid, arbitrarily shaped wheels, which was initially obtained by analyzing RFT system dynamics. The scaling analysis has been reconciled with Coulomb plasticity and an extension has been proposed that could relate locomotion processes in different ambient gravity.

Like RFT itself, our forms neglect rate-sensitivity of the material, which is known to exist (i.e. the  $\mu(I)$  rheology [15, 16]). For more rapidly spinning wheels, this effect could add another degree of complexity to the scaling, however it is plausible the same form will continue to operate suitably for a range of larger speeds, since modifications for rate-dependency change the solution only minimally in many cases [17]. For example, robots that run on sand using “c-legs” [2] move many times their body-length per second yet remain well-described by rate-independent RFT. Other considerations not accounted for by RFT or Coulomb plasticity are the effect of internal texture variables within the deforming granular system and nonlocal effects due to finite grain size. The former suggests that a more complex scaling relationship may be needed to go beyond monotonic driving, e.g. oscillatory wheel motion, but the latter is likely to matter only as wheel feature size competes with the characteristic grain size [18, 19]. We have proposed and tested a scaling relation for rigid wheels, but the scaling could be extended to more complex locomotors with more moving parts by adding additional non-dimensional groups for each new degree of freedom. Testing these extended scaling laws would be important future work.

- (2014).
- [2] C. Li, T. Zhang, and D. I. Goldman, *Science* **339**, 1408 (2013).
  - [3] J. Lighthill, *Mathematical Biofluidynamics* (SIAM, 1975).
  - [4] D. I. Goldman, *Reviews of Modern Physics* **86**, 943 (2014).
  - [5] Y. Ding, N. Gravish, and D. I. Goldman, *Physical review letters* **106**, 028001 (2011).
  - [6] H. Askari and K. Kamrin, arXiv preprint arXiv:1510.02966 (2015).
  - [7] T. Brzinski III, P. Mayor, and D. Durian, *Physical review letters* **111**, 168002 (2013).
  - [8] F. Guillard, Y. Forterre, and O. Pouliquen, *Physics of Fluids (1994-present)* **26**, 043301 (2014).
  - [9] J.-Y. Wong and A. Reece, *Journal of Terramechanics* **4**, 81 (1967).
  - [10] R. B. Ahlvin and P. W. Haley, *Nato Reference Mobility Model: Edition II. NRMM User’s Guide* (US Army Engineer Waterways Experiment Station, 1992).
  - [11] M. G. Bekker, *Theory of Land Locomotion* (University of Michigan Press, 1956).
  - [12] R. M. Nedderman, *Statics and Kinematics of Granular Materials* (Cambridge University Press, 1992).
  - [13] C. Senatore and K. Iagnemma, *Journal of Terramechanics* **51**, 1 (2014).
  - [14] T. Kobayashi, Y. Fujiwara, J. Yamakawa, N. Yasufuku, and K. Omine, *Journal of Terramechanics* **47**, 261 (2010).
  - [15] F. da Cruz, S. Emam, M. Prochnow, J. Roux, and F. Chevoir, *Phys. Rev. E* **72**, 021309 (2005).
  - [16] P. Jop, Y. Forterre, and O. Pouliquen, *Nature* **441**, 727 (2006).
  - [17] P.-Y. Lagrée, L. Staron, and S. Popinet, *Journal of Fluid Mechanics* **686**, 378 (2011).
  - [18] K. Kamrin and G. Koval, *Phys. Rev. Lett.* **108**, 178301 (2012).
  - [19] K. Kamrin and D. L. Henann, *Soft matter* **11**, 179 (2015).

\* Electronic address: kkamrin@mit.edu

[1] J. D. Goddard, *Applied Mechanics Reviews* **66**, 050801